IEEE Access
Multidisciplinary | Rapid Review | Open Access Journal

Received 12 April 2023, accepted 12 May 2023, date of publication 22 May 2023, date of current version 12 July 2023.

Digital Object Identifier 10.1109/ACCESS.2023.3278592

RESEARCH ARTICLE

Active De-Excitation System Using Magnetically Coupled Secondary Coil and Charged Capacitor for Fault Protection of Superconducting Coils

YOJONG CHOI[1], SEUNGHYUN SONG[1], MYUNG SU KIM[1], JAE YOUNG JANG[2], AND YEON SUK CHOI[1]

[1]Center for Scientific Instrumentation, Korea Basic Science Institute, Daejeon 34133, South Korea
[2]School of Electrical, Electronics and Communication Engineering, Korea University of Technology and Education (KOREATECH), Cheonan 31253, South Korea

Corresponding author: Yeon Suk Choi (ychoi@kbsi.re.kr)

This work was supported by the Korea Basic Science Institute (KBSI) under Grant D300200.

ABSTRACT Coils excited for high magnetic fields have large discharging time constants owing to high inductance and low resistance for large operating currents. This type of coil requires a de-excitation system to reduce the current as quickly as possible when a fault occurs and to minimize the damage caused by Ohmic heating. This paper introduces a new de-excitation system that rapidly reduces the current discharged through the dump resistor by using the active current of the secondary coil. To verify the performance of the proposed method, a de-excitation system utilizing the primary superconducting coil and secondary copper coil was constructed and discharging tests were performed. Good agreement was obtained between the circuit simulation and test results. The performance of the proposed system was compared with those of other de-excitation systems, and it was confirmed that the proposed approach provides a feasible and powerful means of reducing the fault energy load and that it reduces this load more than the other systems considered. In addition, the effects of the charging voltage, coupling coefficient, capacitor bank configuration, and diode on the performance of the de-excitation system were analyzed and information about the secondary section that most effectively reduces the current was obtained.

INDEX TERMS Circuit analysis computing, coupled mode analysis, de-excitation system, discharging circuit, fault energy load, protection circuit, quench protection, superconducting coil.

I. INTRODUCTION

Excitation coils are used to generate large magnetic fields instead of permanent magnets in apparatus in which magnetic fields are employed, such as motors, generators, accelerators, and nuclear magnetic resonance devices [1], [2], [3], [4], [5]. The magnetic field magnitude produced by excitation coil is increasing [6], [7], [8]. In order to generate a larger magnetic field, the number of turns and size of the coil are increased, and coils that use low resistances to carry large currents have high ratio of inductance to resistance. In particular, because a high-field superconducting coil has a high operating current density as well as a large discharge time constant [9], [10], [11], the heat generated by Ohmic heating can damage the coil system when a normal zone occurs in any part of a superconducting coil [12], [13], [14]. Therefore, this type of coil requires additional de-excitation systems to extract the energy from inside the coil quickly and protect the coil [13], [15], [16], [17], [18]. When a fault occurs, a resistor is placed into the discharge circuit to reduce the discharge time constant. Although the size of the dump resistor must be increased to promote the coil current decrease, a terminal voltage is produced across the coil equivalent to the product of the parallel resistance and the current through the coil. Because the voltage generated at this time may deteriorate the insulation performance of

The associate editor coordinating the review of this manuscript and approving it for publication was Cihun-Siyong (Alex) Gong.

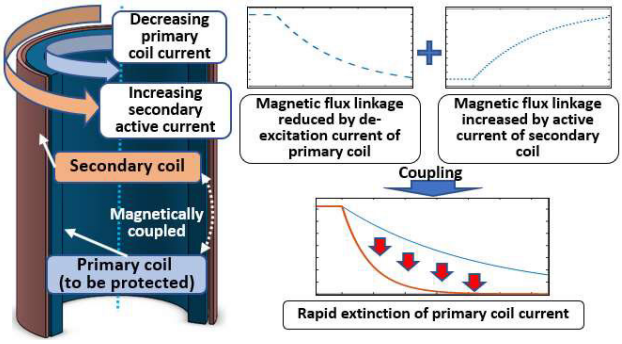

FIGURE 1. Simplified concept of the developed active de-excitation system using a magnetically coupled secondary coil.

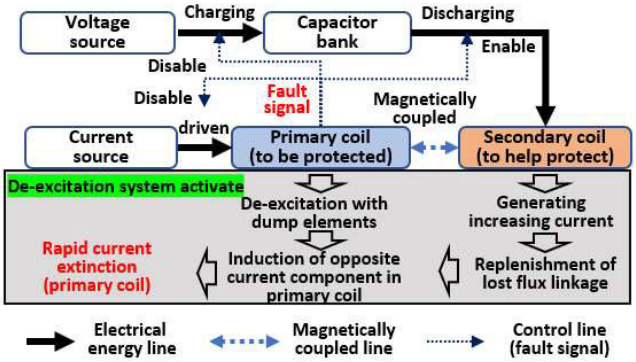

FIGURE 2. Operation flow of the proposed de-excitation system.

the coil or even cause insulation breakdown, the size of the dump resistance is limited [19], [20]. Instead of the parallel resistance, a quench heater (QH) that increases the series resistance inside the coil can be used [21], [22], [23]. However, QHs rely on thermal diffusion across insulation layers; thus, they are inherently slow and can be massive when covering a large percentage of the coil surface [19], [24]. In addition, a QH can be damaged by mechanical friction and may cause electrical breakdown. Therefore, studies have been conducted to develop de-excitation systems for faster current reduction. CERN generated an AC field to increase the series resistance and reduce the energy load to around 85% [19], [25]. Another approach involved switching parallel dump resistors to maintain voltage, reducing fault energy to approximately 40% [26]. A varistor was also studied for protection, which exhibited similar performance to the resistance switching method [26], [27], [28]. In addition, an auxiliary method using a magnetically coupled secondary coil instead of a means of directly increasing the resistance is being studied [29], [30]. This method can facilitate energy dissipation by enabling the secondary coil current to flow through the resistance in the secondary coil when the primary coil is discharged. However, in this method, the energy consumption is determined by the magnitude of the induced secondary current. To achieve meaningful protection, the resistance of the secondary coil must be very low, and both coils should be well-coupled [15]. When the resistance is small, a large amount of current is induced, which may require the use of a metal with lower electrical conductivity than copper to reinforce mechanical strength [31]. To the best of our knowledge, there is no reported case of reducing the quench energy by less than a quarter without exceeding the voltage.

Therefore, to address faults in high-energy excitation coils, a protection system with a new approach is required to rapidly dissipate current and significantly reduce fault energy loads. This paper proposes an additional de-excitation system that injects active current into the magnetically coupled secondary coil to generate counter-electromotive force in the primary coil, eliminating the current from the primary coil more quickly. To verify the proposed de-excitation method, a protection system using a superconducting coil and secondary copper coil was constructed and a de-excitation test was performed. The measured active de-excitation performance was compared with that resulting from using only the dump resistor and secondary passive current. In addition, the effects of the charging voltage, coupling coefficient, capacitor bank configuration, and dump diode on the performance of the proposed de-excitation system were measured and analyzed. The analysis results provide insight into the system configuration and design for applying the proposed de-excitation system to target coils.

II. ACTIVE DE-EXCITATION SYSTEM FOR FAULT PROTECTION

A. MAIN CONCEPT OF DE-EXCITATION SYSTEM

The proposed active de-excitation system is used together with a dump resistor and magnetically coupled secondary coil. When a fault occurs in the coil to be protected, the power supply and coil are separated, and the energy stored in the coil is consumed by the dump resistor in the form of a current. In the discharge of the RL system, a large dump resistor has a small time constant and can decrease the current rapidly, but the size of the dump resistor is limited because of the coil terminal voltage generated by the product of the resistance and the current. Therefore, instead of increasing the resistance, a method of increasing the rate of reduction of the primary coil current using the energy consumed by the current induced in the secondary coil is also employed. The proposed de-excitation system utilizes a method of injecting active current into the secondary coil to counteract the current by generating an opposing electromotive force in the primary coil, unlike the method of consuming additional energy by using the passive induced current of the secondary coil. Fig. 1 provides a schematic of a de-excitation system using magnetically coupled secondary coils and active current. The primary coil to be protected and the secondary coil located outside are magnetically coupled without electrical contact, and the key idea of this de-excitation system using magnetic coupling of the two coils is described by the following

Faraday electromagnetic induction law:

$$\varepsilon(t) = -\left(\frac{d\lambda_1(t)}{dt} + \frac{d\lambda_{12}(t)}{dt}\right) \quad (1)$$

$$\lambda_{12}(t) = k\sqrt{L_1 L_2} \cdot i_2(t) \quad (2)$$

where $\varepsilon(t)$ is the electromotive force of the primary coil; $\lambda_1(t)$ is the magnetic flux linkage generated by the primary coil; $\lambda_{12}(t)$ is the primary coil flux linkage generated by the secondary coil; k is the coupling coefficient; L_1 and L_2 are the self-inductances of the primary and secondary coils, respectively; and $i_2(t)$ is the current of the secondary coil. When the direction of the active current through the secondary coil is the same as that of the dump current of the primary coil, $k\sqrt{L_1 L_2}$ has a positive value. $\lambda_1(t)$ is reduced by the de-excitation current and appears as a component of the positive electromotive force. When $\lambda_{12}(t)$ increases, a negative electromotive force occurs in the primary coil, which means that an electromotive force occurs to create an increasing flux linkage. Thus, increasing the secondary coil current can result in more rapid reduction of the primary coil current, while simultaneously offsetting the primary coil voltage. To obtain a larger counter electromotive force through (1) and (2), a high coupling coefficient k or a rapid increase in the secondary coil current is required.

B. PROTECTION SYSTEM STRUCTURE

Unlike the method using only the shorted secondary coil, the proposed de-excitation method using active current can rapidly increase the secondary active current even if the resistance of the secondary coil is high or the coupling coefficient is not large; therefore, the current of the primary coil is rapidly dissipated. A power supply with a high capacity may be used to generate the current of the secondary coil, as the current of the secondary coil must be significantly increased in a short time to remove the current from the primary coil quickly. Because it is undesirable to always have a high capacity power supply to standby for fault protection, we adopted a method of charging a capacitor and discharging it to the secondary coil instead of supplying current via the power supply. Fig. 2 shows the operation flow of the de-excitation system that injects current into the secondary coil using a charged capacitor bank. In the normal state, the primary coil, which is the coil to be protected, is operated with the current source connected, and the capacitor bank is charged with the connected voltage source. When a fault signal requiring de-excitation is detected in the primary coil, the primary coil is separated from the current source, and de-excitation is initiated through the dump elements. Simultaneously, the capacitor bank is disconnected from the voltage source and connected to the secondary coil to discharge the charged charge. The secondary coil current is generated owing to the discharge of the capacitor, and the flux linkage reduced by the dump in the primary coil is supplemented. Consequently, an electromotive force is generated to suppress the increase in the flux linkage change in the primary coil, causing a decrease in current.

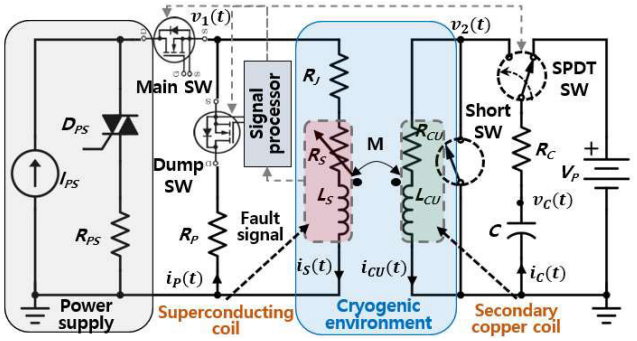

FIGURE 3. Equivalent circuit of the new active de-excitation system with a secondary coupled coil.

III. DE-EXCITATION CIRCUIT WITH SECONDARY COUPLED COIL

A. EQUIVALENT CIRCUIT AND DE-EXCITATION SEQUENCE

The time constant of the current discharged through the dump resistor is given by $\tau = L/R$, i.e., the ratio of the inductance to the sum of the coil and dump resistances. Therefore, if the inductance is large or the coil resistance is small, an additional de-excitation system is needed because the decrease in current is slow owing to the large time constant. To verify the feasibility of the proposed de-excitation system effectively, a superconducting coil with a large time constant owing to the extremely small coil resistance was utilized as the primary coil. Fig. 3 shows the equivalent circuit of the de-excitation system in which the primary and secondary coils are combined. This circuit includes a power supply for providing current to the primary coil, parallel resistor for the dump, capacitor for charging and discharging, and voltage source. The signal processor detects the fault signal from the primary coil and sends an operation signal to each switch (SW). Fault detection in high-temperature superconducting magnets typically employs a critical voltage of 1 μV/cm, although various standards can be selected based on the magnet's intended use. After a fault signal is detected, the signal processor controls each switch once in a predetermined sequence, as shown in Fig. 4. Because commercial power supplies contain internal resistances R_{PS} and protection diodes D_{PS}, the main SW is connected in series to the current lead of the power supply to remove the influence of the internal bypass path of the power supply and to separate it completely from the circuit. The primary superconducting coil can be described using the self-inductance L_S and the quench resistance R_S that rapidly increases during a fault. A primary coil with junction resistance R_J is connected in parallel to the dump element. The dump SW, which blocks the current that can flow to the parallel resistor when charging the current of the primary coil and creates a detour when a fault occurs, is connected in series with the dump resistor. The main and dump SWs adopt a power metal-oxide-semiconductor field-effect transistor (MOSFET) with a faster operation time and higher current capacity than mechanical contact SWs. A secondary copper coil with a resistance R_{CU} and self-inductance L_{CU} is

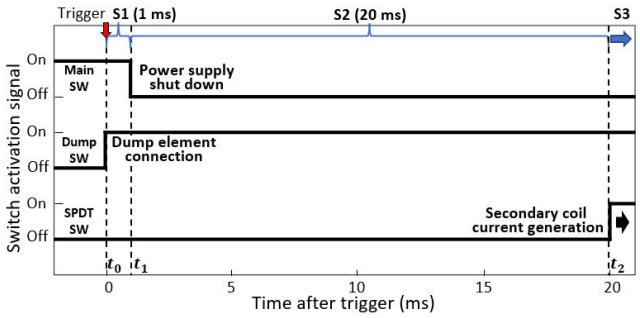

FIGURE 4. Switching sequence during de-excitation system operation.

connected in parallel with a short SW for the passive current test and residual current discharge. The capacitor is charged with V_P, which is the charging voltage of the DC voltage source, and when a fault occurs, the single-pole double-throw (SPDT) SW disconnects the capacitor from the voltage source and connects it to the secondary coil. The two magnetically coupled coils were placed in a cryogenic environment to maintain the superconducting state of the primary coil.

Fig. 4 shows the activation signals delivered to each SW after fault detection. In the normal state before fault detection, the main and dump SWs maintain close and open states, respectively. When a fault is detected, the dump SW is firstly connected during S1 to secure a dump path. When S1 operation is finished and S2 is started, the main SW is opened to disconnect the power supply providing current to the primary coil, and the primary coil current starts dumping with the parallel resistance. When the primary coil is de-excited, the charged capacitor is connected to the secondary coil by the SPDT SW, and S3 operation proceeds. The shorter period S2, the earlier the active current of the secondary coil is generated, resulting in faster de-excitation, but S2 was set to 20 ms in this study to compare clearly the current reduction resulting from using the parallel resistance only with that achieved by employing the secondary coil current.

B. DE-EXCITATION TRANSIENT CHARACTERISTICS

As illustrated in Fig. 4, the system has four-time sections: before triggering, S1, S2, and S3. The normal and transient currents of the primary coil in each session are expressed by the following equations:

$$i_s(t) = I_{PS}, (t < t_0), \tag{3}$$

$$i_s(t) = \frac{I_{PS}}{R_1}\left\{(R_S + R_J)\cdot e^{-\frac{R_1}{L_S}(t-t_0)} + R_P\right\}, \ (t_0 \le t < t_1) \tag{4}$$

$$i_s(t) = i_s(t_1)\cdot e^{-\frac{R_1}{L_S}(t-t_1)}, (t_1 \le t < t_2) \tag{5}$$

where I_{PS} is the normal operating current of the primary coil, R_1 is the combined resistance of the primary side ($R_1 = R_P + R_J + R_S$), and each symbol is described in the equivalent circuit of Fig. 3. During normal operation, the current of the primary coil is maintained at I_{PS} using a constant current source. After the de-excitation system is operated, a parallel dump element is connected in parallel to the primary coil, and the current of the power supply is distributed to the coil and parallel branches according to the resistance ratio. At this time, a transient current with a time constant of $L_S/(R_P + R_J + R_S)$, as expressed in (4), is included. When the main SW is opened and the power supply is disconnected, the current of the primary coil is expressed by (5) and is dumped in the form of natural discharge according to the RL ratio. The primary and secondary coil currents during period S3 in which the charged capacitor is discharged to the secondary coil are calculated by applying the following the simultaneous circuit equation:

$$\begin{cases} L_S\dfrac{di_S(t-t_2)}{dt} + M\dfrac{di_{CU}(t-t_2)}{dt} \\ +(R_S)\,i_s(t-t_2) = 0 \\ L_{CU}\dfrac{di_{CU}(t-t_2)}{dt} + M\dfrac{di_S(t-t_2)}{dt} \\ +(R_C + R_{CU})\,i_{CU}(t-t_2) \\ +\dfrac{1}{C}\displaystyle\int_{t_2}^{t-t_2} i_{CU}(t)dt + v_C(t_2) = 0, \\ (t_2 \le t), \end{cases} \tag{6}$$

where M is the mutual inductance of the primary and secondary coils, v_C is the voltage across the capacitor, and R_C is the equivalent series resistance (ESR) of the capacitor. A solution of (6) in which $i_s(t)$ decreases as $i_{CU}(t)$ increases can be calculated using a numerical analysis method. When S3 begins, the current of the secondary coil decreases after increasing owing to the RLC transient characteristic, and the generated current has an RLC damping characteristic. Because the resistance of the secondary copper coil is much larger than that of the primary superconducting coil, the damping ratio of the secondary coil current can be simplified as follows:

$$\xi = \frac{C\cdot R_2^2}{4L_{CU}}, \tag{7}$$

where R_2 is the combined resistance of the secondary side, including the coil resistance ($R_2 = R_{CU} + R_C$) and the ESR of the capacitor. Because the decreasing current of the secondary coil increases the current of the primary coil, in order to maximize the effect of reducing the current of the primary coil, the current of the secondary coil should increase rapidly and, conversely, decrease slowly. This transient response is overdamping with a damping ratio greater than 1 in (7), and the overdamping current of the secondary coil is represented by the following equations:

$$i_{CU}(t) = A\cdot\left(e^{-\frac{t}{\tau_d}} - e^{-\frac{t}{\tau_r}}\right) \tag{8}$$

$$A = \frac{V_P}{\sqrt{R_2^2 - \frac{4L_{CU}}{C}}} \tag{9}$$

$$\tau_r = 2/\left(\frac{R_2}{L_{CU}} + \sqrt{\left(\frac{R_2}{L_{CU}}\right)^2 - \frac{4}{L_{CU}C}}\right) \tag{10}$$

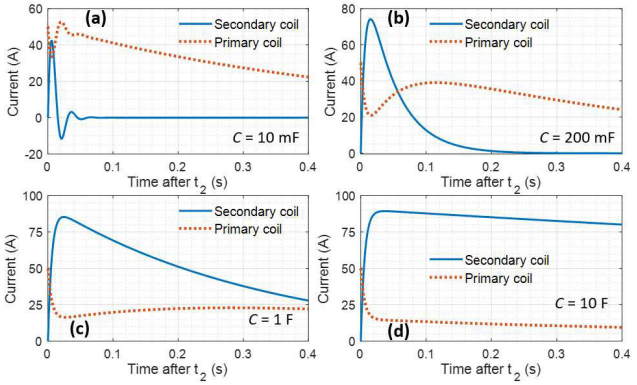

FIGURE 5. Primary and secondary coil currents calculated according to the damping characteristics. (a) Underdamping ($\xi < 1$); (b) critical damping ($\xi = 1$); (c) over damping ($\xi > 1$); (d) overdamping ($\xi \gg 1$).

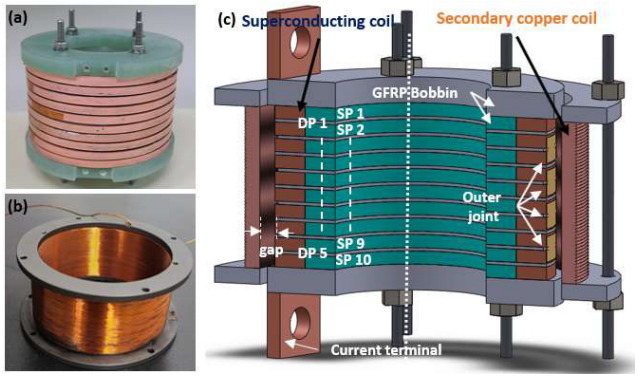

FIGURE 6. (a) Manufactured superconducting coil; (b) manufactured bobbin-free copper coil; (c) assembly schematic diagram of superconducting coil and secondary copper coil.

$$\tau_d = 2/\left(\frac{R_2}{L_{CU}} - \sqrt{\left(\frac{R_2}{L_{CU}}\right)^2 - \frac{4}{L_{CU}C}}\right) \tag{11}$$

where τ_r is the increasing time constant and τ_d is the decreasing time constant. According to the equations for the two time constants, in order to reduce the increasing time constant and increase the decreasing time constant, a larger capacitance is advantageous, as it satisfies $C > 4L_{CU}/R_2^2$. Fig. 5 presents the numerical solutions of the various damping characteristics of (6) according to the capacitance values using arbitrary inductance and resistance values. As shown in Fig. 5a, when the capacitance is low, under-damping, which is an oscillating current, occurs, and the current of the primary coil repeatedly decreases and increases, so the effect of reducing the current is very small. Fig. 5b demonstrates that the current at the critical damping that reaches the steady state is the fastest. The increasing rate of the secondary coil current is fast. However, the decreasing rate is also fast. As a result, the primary coil current decreases and then increases. Figs. 5c and d show the over-damping current, which increases and then decreases slowly. Because the slow rate of decrease of the secondary current reduces the effect of increasing the primary coil current, the larger the capacitance, the slower the rate of decrease of the secondary coil current, suppressing the repeated increase in the primary coil current.

C. FAULT ENERGY LOAD FOR SYSTEM PERFORMANCE EVALUATION

When a superconducting coil exceeds a critical temperature, critical current, or critical magnetic field, a fault called quench occurs, which corresponds to a change from a superconducting state to a normal conducting state. When a quench occurs, the resistance of the superconductor is calculated using the E-J power law using the following equation:

$$R_S(t) = \frac{E_0}{I_C(T)}\left(\frac{i_S(t)}{I_C(T(t))}\right)^{n-1}, \tag{12}$$

where E_0 is the critical quench voltage of 1 uv/cm, $i_S(t)$ is the current of the superconducting wire, and n is the index value of the E-J power law. $I_C(T)$ is the linearly approximated critical current, which decreases with increasing temperature and is obtained from the following equation:

$$I_c(T) = \frac{I_{C0}}{T_C - 77.3}(T_C - T), \tag{13}$$

where I_{C0} is the critical current at 77.3 K and T_C is the critical temperature of the superconducting wire. Because the index of a high-temperature superconducting wire is 20–40 [32], [33], when the quench starts after fault occurrence, the resistance and temperature increase rapidly. When a quench occurs, the following thermal equilibrium equation is satisfied under adiabatic conditions:

$$I_c(T) = \frac{I_{C0}}{T_C - 77.3}(T_C - T), \tag{14}$$

where $\rho(T)$ is the resistivity according to the temperature of the superconductor, $J(t)$ is the current density of the superconducting wire, γ is the area of the wire, and $C(T)$ is the heat capacity. If the temperature term is transposed to the right side, only the integral of the square of the current remains on the left side, and the final temperature increase of the coil is proportional to the integral of the square of the current. To compare the effects of the decrease in current on the temperature increase in various de-excitation systems, the integral of the square of the current was defined as the fault energy load instead of the accurately calculated increase in temperature and used as an evaluation criterion.

IV. MEASURED FAULT PROTECTION SYSTEM BEHAVIORS

A. EXPERIMENTAL SETUP

For experimental verification of the proposed de-excitation system, a primary superconducting coil and secondary copper coil were fabricated, as shown in Figs. 6a and b. The superconducting coil was wound using 4.1-mm-wide 2G GdBCO tape with a critical current of 160 A or more. The secondary coil was wound using enameling copper wire with a diameter of 1 mm. To increase the coupling coefficient by placing the two coils as close together as possible, a secondary coil surrounding the primary coil was manufactured using the

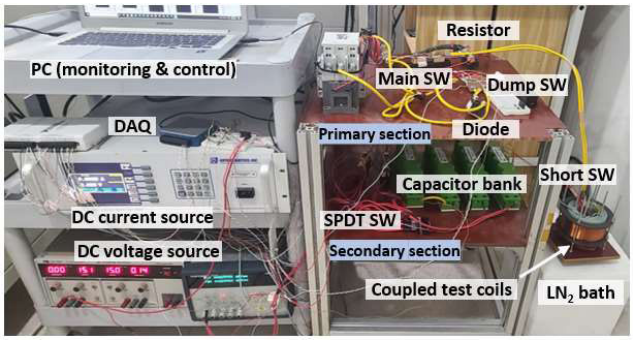

FIGURE 7. Complete system configuration for de-excitation testing in liquid nitrogen.

bobbin-free winding technique. Fig. 6c shows a schematic diagram of the cross-section of the two coils combined. The primary superconducting coil was constructed by stacking five double pancake coils (DPCs) with two single pancake coils inner jointed, and the connection between the neighboring DPCs was externally joined using superconducting tape, which was 8 mm wide. The gap between the primary and secondary coils was 5 mm, and Table 1 summarizes the specifications of the two manufactured coils. The primary and secondary coils were insulated with Kapton tape and epoxy, respectively, and were constructed at the same height. The critical current of the primary superconducting coil was measured at 58.78 A, and the normal operating current was set at 50 A, which is 85% of the critical current. The numbers of turns in the two coils were 530 and 232, and the self-inductance of the primary coil was measured to be 17.40 mH, which was three times that of the secondary coil. When the two coils were placed at the same height as the concentric axis, the mutual inductance and coupling coefficients were measured and calculated to be 7.00 mH and 0.7009, respectively. Fig. 7 shows the configuration of the entire system configured for the de-excitation experiment. To maintain the superconducting state of the primary coil, a performance test was conducted in a liquid nitrogen bath, and the secondary coil was cooled to 77 K, the temperature of liquid nitrogen. The self-inductance of the secondary copper coil was calculated to be 5.73 mH, and the electrical resistance in the 77 K liquid nitrogen bath was measured to be 208.96 mΩ. Thus, the minimum capacitance necessary to satisfy the over-damped condition in (7) was calculated to be 0.43 F. A supercapacitor module with an allowable voltage of 18 V and capacitance of 61.7 F was used to configure the capacitor bank. Therefore, depending on the number of capacitance connections, the capacitance can be adjusted in four steps from 15.4 F to 61.7 F, and the maximum chargeable voltage can be adjusted in four steps from 18 V to 72 V. A DC current source to excite the primary coil, a DC voltage source to charge the capacitor, and another DC voltage source to control each SW were installed. Each SW was controlled by a solid-state relay and an analog output module included in the data acquisition system. An N-channel enhancement

TABLE 1. Specifications of superconducting coil and secondary copper coil manufactured for de-excitation test.

Primary superconducting coil	
Inner/outer diameter	70/90 mm
Number of DPCs/SPCs	5/10 EA
Turns per SPC	53
Height	50 mm
Critical current @77 K	58.78 A
Winding length	139.31 m
Self-inductance	17.40 mH
Turn to turn insulator	Kapton tape
Secondary copper coil	
Inner/outer diameter	100/110 mm
Number of turns	232
Wire diameter/winding length	1.02/76,158 mm
Height	50 mm
Coil resistance @77 K	208.96 mΩ
Self-inductance	5.73 mH
Turn to turn insulator	Stycast 2850
Magnetically coupling relationship	
Gap	5 mm
Mutual inductance	7.00 mH
Coupling coefficient	0.7009

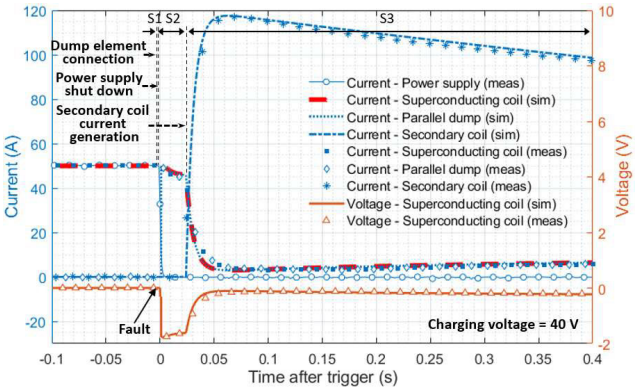

FIGURE 8. Current of each element and voltage of the primary superconducting coil resulting from the operation of the de-excitation system.

mode power MOSFET with a capacity of 660 A, turn-on time of 40 ns, and turn-off time of 386 ns was selected for the main and dump SWs, and a high current relay with a current switching capability of 300 A was used for the SPDT SW. In addition, the secondary coil terminal was equipped with a short SW to configure a protection system using a passive current.

B. MEASUREMENT OF DE-EXCITATION SYSTEM BEHAVIORS

The current was measured using shunt resistors installed on all branches to verify the behavior of the de-excitation systems with the S1 and S2 times set to 1 and 20 ms, respectively. The capacitor bank was configured to have a capacitance of 15 F and was charged to 40 V during normal operation. Fig. 8 shows the currents of all branches and the voltage of the primary coil to be protected before and after the de-excitation

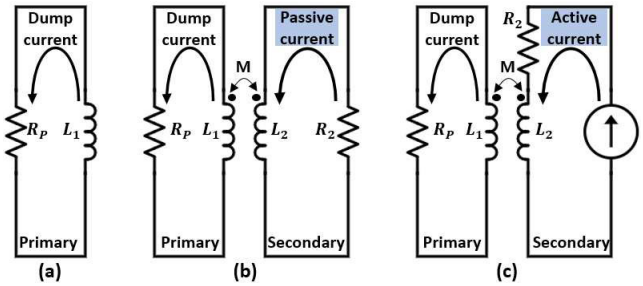

FIGURE 9. Simplified circuit configurations corresponding to several de-excitation methods. (a) Using only the parallel resistor; (b) using a magnetically coupled short-circuited secondary coil; (c) injecting the increasing active current into the secondary coil.

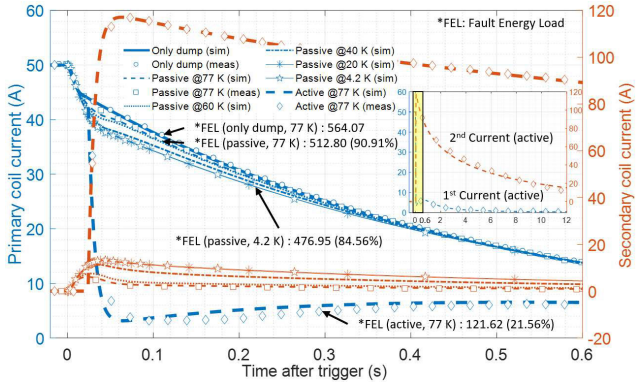

FIGURE 10. Primary and secondary coil currents measured in three protection systems and the passive method simulation results obtained under different operating temperature conditions.

system was triggered. The primary coil was excited with a current of 50 A, and it remained stable without occurrence of quench voltage. Because the duration of S1 after the de-excitation system trigger was very short, at 1 ms, a few transient currents were distributed to parallel resistances by (4), and section S2 was started. During S2, the power supply current was completely cut off and the natural discharge through the dump resistor began, with the primary coil current having a time constant equal to the ratio of resistance to inductance. At this time, the terminal voltage of the primary coil was generated as the product of the parallel resistance and primary coil current. When the charged capacitor was connected to the secondary coil and section S2, where the secondary active current was generated, the secondary coil current increased to the maximum value of 117.5 A in 38 ms and then decreased slowly. The current of the primary coil, which was naturally discharged, was rapidly reduced owing to the secondary active current, and the terminal voltage of the primary coil was also reduced. Manufacturing errors in the arrangement and shapes of the two manufactured coils may cause errors in the coupling coefficient. Because the coupling coefficient calculated from the designed shape was used in the simulation, the measurement and simulation results for the current of the primary superconducting coil differ slightly near the maximum increase point of the secondary coil current, where the slope of the secondary coil current rapidly decreases. However, the currents for the rest of the period were mostly consistent, and the fault energy load was calculated as 121.62 A^2s and 123.39 A^2s from the simulated and measured currents for the entire time, respectively, with an error of 1.43%.

C. COMPARISON WITH OTHER PROTECTION METHODS

For relative evaluation of the performance of this protection system, it was compared with the conventional protection method using the passive current of the secondary coil. Fig. 9 shows the simplified circuit configurations of several de-excitation methods. Fig. 9a depicts the configuration of the most basic method in which the power supply current is cut off and discharged using only the parallel resistor R_P. Fig. 9b illustrates a method of additionally using a short-circuited secondary coil magnetically coupled to the system shown in Fig. 9a. In this configuration, the induced passive current of the secondary coil, which is generated when the current of the primary coil decreases, flows through the secondary coil resistor R_2 to help consume energy. This method requires a well-coupled low-resistivity shorted-secondary coil because a large passive current must be induced in the secondary coil to increase the energy consumption [15], [30]. Fig. 9c shows the proposed method of injecting the increasing active current into the secondary coil. In Fig. 10, the measured and calculated currents of the primary and secondary coils of the three protection methods are compared. The fault energy load of the protection method using only the dump resistor was calculated to be 564.07 A^2s. In the passive protection test performed at 77 K, the current induced in the secondary coil was increased to 5.18 A, and the fault energy load was reduced by 9.09% compared to that obtained from the method using only the dump resistor. As the induced current increases when the resistance of the secondary coil decreases, the secondary passive current generated at 60, 40, 20, and 4.2 K and the corresponding primary coil current were simulated. At 4.2 K, which is the vaporization temperature of liquid helium used to operate the low-temperature superconducting coil, the maximum increase in current of the secondary coil was calculated to be 13.21 A, and fault energy load reduction of 15.44% compared to the dump system was predicted. On the other hand, in the protection test using the active current at 77 K, the secondary coil current was increased to 117.11 A, and the fault energy load was reduced by 78.44% compared to that when only the dump resistor was utilized.

V. EFFECTS OF SYSTEM PARAMETERS ON PROTECTION PERFORMANCE

A. EFFECT OF CHARGING VOLTAGE

The de-excitation performance of the proposed protection system, in which the circuit parameters such as the coupling coefficient, inductance, coupling coefficient, and resistance are fixed, is determined by the increase in the secondary coil current and can be controlled by adjusting the charging voltage of the capacitor. The maximum allowable voltage of

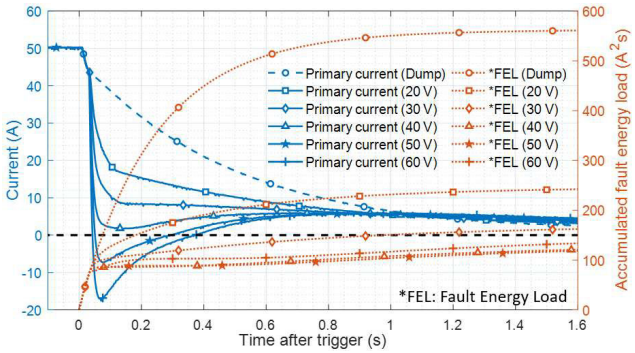

FIGURE 11. Measured current and accumulated fault energy load calculation results of primary coil operated with various charging voltages.

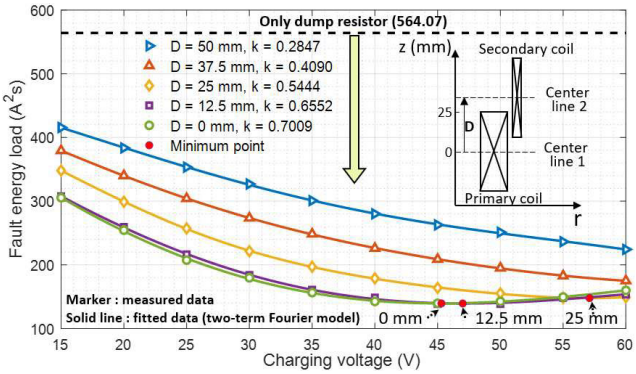

FIGURE 12. Measured fault energy loads of coil arrangements with various coupling coefficients according to charging voltages.

a capacitor bank with four capacitor modules connected in series was calculated to be 72 V, and the voltage source used for charging had an output of up to 60 V. To analyze the effect of the charging voltage, a de-excitation test was performed in which five charging voltages in 10 V intervals from 20 V to 60 V were used considering the allowable voltage of the capacitor bank and the capacity of the voltage source. Fig. 11 shows the measured de-excitation current and accumulated fault energy load for each charging voltage. As the charging voltage increases, the generated secondary coil current increases, and the primary coil current decreases. The higher the charging voltage, the faster the current decreases in the initial large current region, but a counter current is generated above a certain voltage. When charging at 50 V and 60 V, a counter current is produced in the primary coil. Because the generated counter current affects the temperature increase similar to the forward current, the contribution to the temperature increase was evaluated by calculating the accumulated fault energy load. Even at the lowest charging voltage of 20 V, compared to the de-excitation using only the dump resistor, the fault energy load accumulated only 43%. The fault energy load accumulated for 1.6 s was evaluated to be the lowest in the case of charging at 50 V despite the occurrence of a counter current of 7.3 A. Once the coil to be protected is determined, various specifications such as the magnitude of the normal operating current, inductance, and dump resistance are fixed, so the de-excitation performance can be maximized by adjusting the charging voltage.

B. EFFECT OF COUPLING COEFFICIENT

The size and location of the secondary coil that can be installed may be limited depending on the shape and structure of the apparatus in which the coil is used. For example, there may be cases in which only a small secondary coil can be installed because the space for the secondary coil surrounding the primary coil is narrow, or the secondary coil cannot be wrapped around the primary coil and instead must be placed above and below the latter. In these cases, the coupling coefficient between the primary and secondary coils becomes small, and the effect of the secondary coil current on the primary coil is reduced due to the reduced mutual inductance. Therefore, a method of increasing the charging voltage can be considered to overcome the low coupling coefficient. Fig. 12 shows the fault energy load measured by the coupling coefficient and charging voltage. To change the coupling coefficients of the two manufactured coils, the distance in the z-direction between the primary and secondary coils was adjusted, as shown in Fig. 12. Half of the heights of the primary and secondary coils are indicated by center lines 1 and 2, respectively, and the distance between the two center lines is denoted as D. If the center lines coincide, D becomes 0 mm, and the coupling coefficient is 0.7009, which is the largest coupling relation among all configurations. When the z-positions of the bottom of the secondary coil and the top of the primary coil are aligned, D is 50 mm, and the coupling coefficient is 0.2847. The de-excitation current was measured, and the fault energy load was calculated by changing the charging voltage in 5 V intervals from 15 V to 60 V in five arrangements in which D was increased in 12.5 mm increments from 0 mm to 50 mm. Although there is a difference in the fault energy load reduction ratio depending on the charging voltage, when charged at 45 V, the fault energy loads of the cases with coupling coefficients of 0.7009 and 0.2847 were measured to be 139.69 and 262.79 A^2s, respectively, and decreased by 75.24% and 53.41%, respectively, compared to when only the dump resistor was used. In the case of the lowest coupling coefficient of 0.2847, the fault energy load was measured to be 224.18A^2s when charged to the set maximum charging voltage of 60 V and was reduced by 60.26% compared to the dump resistor case. The lower the coupling coefficient, the more the fault energy load can be reduced by increasing the charging voltage, but the fault energy load increases because of the counter current above a certain voltage. The measured data were fitted using a two-term Fourier model, and the minimum fault energy load is indicated by a red dot in Fig. 12. The charging voltages for the maximum reduction of the fault energy load in the arrangements with D of 0, 12.5, and 25 mm were evaluated to be 45.3, 47, and 57.1 V, respectively. Consequently, there is an optimal charging voltage for the minimum fault energy load

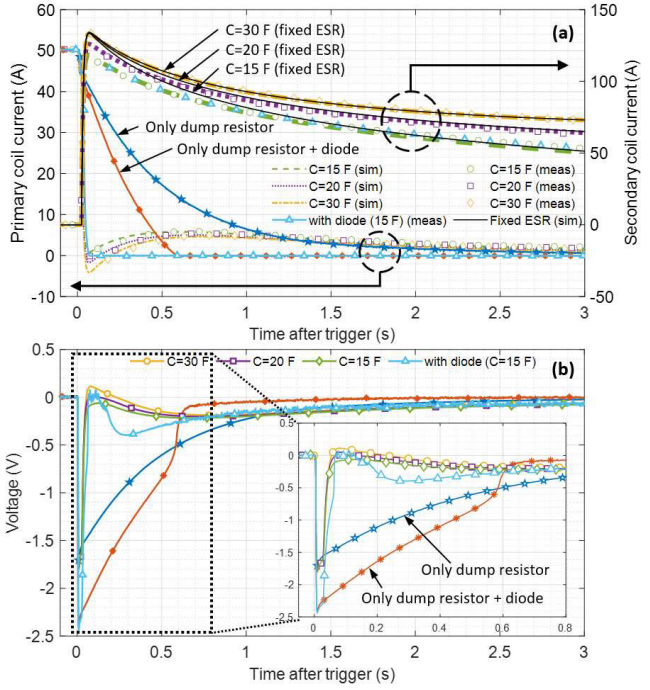

FIGURE 13. Comparison of de-excitation system behavior according to the capacitor bank configuration and the effect of the dump element. (a) Primary and secondary coil currents; (b) primary coil voltage.

for each coupling coefficient, and as the coupling coefficient decreases, the optimal charging voltage increases.

C. EFFECT OF CAPACITOR BANK AND DUMP DIODE

To compare the de-excitation operation characteristics according to the capacitance and ESR, the primary and secondary currents were measured with different capacitor bank configurations, as shown in Fig. 13. Capacitor banks with capacitances of 30, 20, and 15 F were combined using 2 to 4 series connections and a 61.7 F supercapacitor module, and all capacitor banks were charged with 40 V. Fig. 14a presents the currents of the primary and secondary coils measured for each capacitor bank configuration. In the case of 30 F, where two capacitor modules were connected, the current of the secondary coil increases the most, and in the case of 15 F, where four capacitor modules were connected, the current of the secondary coil increases the least. The fault energy loads of the system using 15, 20, and 30 F capacitance bank combinations were measured to be 143.60, 131.23, and 124.31 A^2s, respectively. Because the ESR of one capacitor module is 22 mΩ, the total ESR is also multiplied times the number of connections when the number of series connections is increased. When four capacitor modules are connected in series, the ESR is increased to 88 mΩ, so it contributes 42% of the resistance of the secondary coil (208.96 mΩ measured at 77 K). To compare the contributions of the capacitance and ESR, the ESR of the capacitor bank was fixed at 22 mΩ, and the currents in the primary and secondary coils according to each capacitance were simulated and are indicated by the black solid line in Fig. 13. The simulation results show that the maximum value of the secondary current does not differ significantly depending on the capacitance, but rather only the rate of decrease varies. Therefore, the difference in ESR, rather than capacitance, was analyzed as the main cause of the increase in the measured secondary current. Consequently, the maximum current was observed when the overall ESR was the smallest for the 30 F case because the number of serial connections in the capacitor was the smallest in this situation. Therefore, it is more important to configure an ESR smaller than to increase the capacitance of the capacitor bank to increase the maximum current of the secondary coil with a small resistance.

The diode connected in parallel with the coil is turned on when the voltage exceeds the threshold voltage due to a fault, and the current is passively dumped. Owing to the passive dump function, a diode can be used with a parallel resistor as a dump element. To analyze the performance of the system in which the diode is added, a diode with a threshold voltage of 0.85 V was inserted into the parallel branch. Fig. 13a presents the measured currents of the coils when only the dump resistor is used, a diode is added, the diode and secondary active current are used together. The sum of the turn-on resistance of the diode and the resistance of the connecting line was measured to be 14.34 mΩ, indicating that the total dump resistance of the branch including the diode was increased. Therefore, the current decreased faster because it had a smaller time constant than in the system using only parallel dump resistors. However, as shown in Fig. 13b, the resistance of the diode itself was added to the parallel branch, resulting in a larger terminal voltage. In the system in which the diode and secondary active current are used together, as the primary current decreases, the coil terminal voltage becomes lower than the threshold voltage (0.85 V), and the diode turns off. When the secondary coil current decreases, the induced primary coil voltage does not exceed the diode threshold voltage; therefore, the current path does not exist. Therefore, the primary coil current does not increase again despite the decrease in the secondary coil current after reaching 0 A.

VI. CONCLUSION

To overcome the resistance increase limitations imposed by the generated voltage and low passive induced current of the secondary coil, a new de-excitation system using the active current of the secondary coil was developed to remove the current quickly when a fault occurs. To verify the feasibility of the proposed method experimentally, a de-excitation system was constructed and tested successfully. The simulated and experimentally measured fault energy loads agreed closely, and it was confirmed that the currents of all the branches fit the test results well. Compared to the conventional method using only a dump resistor that generated a fault energy load of 564.07 A^2s, the protection system using the passive current reduced the fault energy load to 512.80 A^2s, but the proposed active de-excitation system significantly reduced the load to 121.62 A^2s, which means that the fault

stability was increased by 78.44%. A secondary coil was built with 66% of the volume and 44% of the winding of the superconducting coil. To reduce the volume of the secondary coil, the coupling coefficient or the current of the secondary coil can be increased. Experimental analysis was performed to evaluate the impact of the coupling coefficient and charging voltage on de-excitation damping efficiency. The analysis results provide insights into achieving the best de-excitation performance. The proposed system can be used with the existing de-excitation method to remove energy faster and can help suppress the rapid temperature increase of a faulty coil by reducing the fault energy load.

REFERENCES

[1] F. Milan and M. Anghel, "Impact of time delays on power system stability," *IEEE Trans. Circuits Syst. I, Reg. Papers*, vol. 59, no. 4, pp. 889–900, Apr. 2012, doi: 10.1109/TCSI.2011.2169744.

[2] S. Hong and N. Sun, "A portable NMR system with 50-kHz IF, 10-us dead time, and frequency tracking," in *Proc. IEEE Symp. VLSI Circuits*, Jun. 2020, pp. 1–2, doi: 10.1109/VLSICircuits18222.2020.9163029.

[3] A. Den Ouden and S. Wessel, "Application of Nb_3Sn superconductors in high-field accelerator magnets," *IEEE Trans. Appl. Supercond.*, vol. 7, no. 2, pp. 733–738, Jun. 1997, doi: 10.1109/77.614608.

[4] X. Zhu and M. Cheng, "Design and analysis of 10 MW class HTS exciting double stator direct-drive wind generator with stationary seal," *IEEE Access*, vol. 7, pp. 51129–51139, 2019, doi: 10.1109/ACCESS.2019.2911298.

[5] H. Park and M. Lim, "Design of high power density and high efficiency wound-field synchronous motor for electric vehicle traction," *IEEE Access*, vol. 7, pp. 46677–46685, 2019, doi: 10.1109/ACCESS.2019.2907800.

[6] M. Schlamann, M.-S. Yoon, S. Maderwald, T. Pietrzyk, A. K. Bitz, M. Gerwig, M. Forsting, S. C. Ladd, M. E. Ladd, and O. Kastrup, "Short term effects of magnetic resonance imaging on excitability of the motor cortex at 1.5 T and 7 T," *Academic Radiol.*, vol. 17, no. 3, pp. 277–281, Mar. 2010, doi: 10.1016/j.acra.2009.10.004.

[7] O. P. Mahela, N. Gupta, M. Khosravy, and N. Patel, "Comprehensive overview of low voltage ride through methods of grid integrated wind generator," *IEEE Access*, vol. 7, pp. 99299–99326, 2019, doi: 10.1109/ACCESS.2019.2930413.

[8] A. Bergen, R. Andersen, M. Bauer, and H. Boy, "Design and in-field testing of the world's first ReBCO rotor for a 3.6 MW wind generator," *Supercond. Sci. Technol.*, vol. 32, no. 12, 2019, Art. no. 125006.

[9] I. Song, A. Roshal, V. Tanchuk, J. Thomsen, F. Milani, and I. Benfatto, "The fast discharge system of ITER superconducting magnets," in *Proc. Int. Conf. Electr. Mach. Syst.*, Aug. 2011, pp. 1–6, doi: 10.1109/ICEMS.2011.6073779.

[10] V. Klyukhin, B. Curé, N. Amapane, A. Ball, A. Gaddi, H. Gerwig, A. Hervé, R. Loveless, and M. Mulders, "Using the standard linear ramps of the CMS superconducting magnet for measuring the magnetic flux density in the steel flux-return yoke," *IEEE Trans. Magn.*, vol. 55, no. 2, pp. 1–4, Feb. 2019, doi: 10.1109/TMAG.2018.2868798.

[11] K. Risse, T. Rummel, T. Mönnich, F. Füllenbach, and H.-S. Bosch, "Updates on protection system for Wendelstein 7-X superconducting magnets," *Fusion Eng. Design*, vol. 146, pp. 910–913, Sep. 2019, doi: 10.1016/j.fusengdes.2019.01.111.

[12] S. Chigusa, H. Maeda, Y. Taniguchi, N. Hayakawa, and H. Okubo, "Insulation performance of pressurized liquid helium under quench-induced thermal bubble disturbance for superconducting power apparatus," *IEEE Trans. Dielectr. Electr. Insul.*, vol. 6, no. 3, pp. 385–392, Jun. 1999, doi: 10.1109/94.775627.

[13] N. Nanato, Y. Tsumiyama, S. B. Kim, S. Murase, K.-C. Seong, and H.-J. Kim, "Development of quench protection system for HTS coils by active power method," *Phys. C, Supercond. Appl.*, vols. 463–465, pp. 1281–1284, Oct. 2007, doi: 10.1016/j.physc.2007.02.047.

[14] T. Yamaguchi, E. Ueno, T. Kato, and K. Hayashi, "Quench protection of DI-BSCCO coil," *Phys. Proc.*, vol. 65, pp. 225–228, Jan. 2015, doi: 10.1016/j.phpro.2015.05.126.

[15] M. A. Green, "Various quench protection methods for HTS magnets," in *Proc. IOP Conf. Mater. Sci. Eng.*, vol. 755, Jun. 2020, Art. no. 012134, doi: 10.1088/1757-899X/755/1/012134.

[16] Changjiang Water Resources Commission, Design and Research Institute, "Discussion on the technical requirements of de-excitation system for generators," *Dam Observ. Geotech. Tests*, vol. 3, no. 1, pp. 1–7, 2005, doi: 10.2320/materia.44.24.

[17] K. Wang, Z. Song, P. Fu, W. Tong, H. Li, and X. Zhang, "Structure optimization of fast discharge resistor system for quench protection system," *IEEE Access*, vol. 7, pp. 52122–52131, 2019, doi: 10.1109/ACCESS.2019.2911710.

[18] W. Tong, H. Li, P. Fu, Z. Song, K. Wang, S. Wang, and X. Zhang, "Parameter optimization of thyristor snubber circuit in LSTF quench protection system," *IEEE Access*, vol. 7, pp. 81257–81265, 2019, doi: 10.1109/ACCESS.2019.2923442.

[19] E. Ravaioli, V. I. Datskov, C. Giloux, G. Kirby, H. H. J. Ten Kate, and A. P. Verweij, "New, coupling loss induced, quench protection system for superconducting accelerator magnets," *IEEE Trans. Appl. Supercond.*, vol. 24, no. 3, pp. 1–5, Jun. 2014, doi: 10.1109/TASC.2013.2281223.

[20] L. Coull, D. Hagedorn, V. Remondino, and F. Rodriguez-Mateos, "LHC magnet quench protection system," *IEEE Trans. Magn.*, vol. 30, no. 4, pp. 1742–1745, Jul. 1994, doi: 10.1109/20.305593.

[21] F. Rodriguez-Mateos and F. Sonnemann, "Quench heater studies for the LHC magnets," in *Proc. Part. Accel. Conf.*, 2001, pp. 3451–3453, doi: 10.1109/PAC.2001.988141.

[22] A. V. Fernández and F. Rodríguez-Mateos, "Reliability of the quench protection system for the LHC superconducting elements," *Nucl. Instrum. Methods Phys. Res. A, Accel. Spectrom. Detect. Assoc. Equip.*, vol. 525, no. 3, pp. 439–446, Jun. 2004, doi: 10.1016/j.nima.2004.01.081.

[23] A. V. Dudarev, A. V. Gavrilin, H. H. J. T. Kate, D. E. Baynham, M. J. D. Courthold, and C. Lesmond, "Quench propagation and protection analysis of the ATLAS toroids," *IEEE Trans. Appiled Supercond.*, vol. 10, no. 1, pp. 365–368, Mar. 2000, doi: 10.1109/77.828249.

[24] E. Ravaioli, H. Bajas, V. I. Datskov, V. Desbiolles, J. Feuvrier, G. Kirby, M. Maciejewski, H. H. J. T. Kate, A. P. Verweij, and G. Willering, "First implementation of the CLIQ quench protection system on a full-scale accelerator quadrupole magnet," *IEEE Trans. Appl. Supercond.*, vol. 26, no. 3, pp. 1–5, Apr. 2016, doi: 10.1109/TASC.2016.2529840.

[25] E. Ravaioli, V. I. Datskov, G. Kirby, H. H. J. T. Kate, and A. P. Verweij, "A new hybrid protection system for high-field superconducting magnets," *Superconductor Sci. Technol.*, vol. 27, no. 4, Mar. 2014, Art. no. 044023, doi: 10.1088/0953-2048/27/4/044023.

[26] S. Chen, Q. Wang, Y. Dai, Y. Lei, and K. Kim, "Development of a digital quench detection and dumping circuit with constant voltage system for SMES," *IEEE Trans. Appl. Supercond.*, vol. 20, no. 3, pp. 2070–2073, Jun. 2010, doi: 10.1109/TASC.2010.2043242.

[27] B. P. Strauss and M. A. Green, "Varistors: A useful tool for superconducting magnet quench protection," *IEEE Trans. Appl. Supercond.*, vol. 31, no. 5, pp. 1–5, Aug. 2021, doi: 10.1109/TASC.2021.3058225.

[28] M. A. Green, "The effect of shorted secondary circuit material on quench protection of an HTS tape solenoid discharged across a varistor," in *Proc. IOP Conf. Mater. Sci. Eng.*, vol. 755, no. 1, 2020, Art. no. 012127, doi: 10.1088/1757-899X/755/1/012127.

[29] S. An, K. Choi, J. Bang, U. Bong, and S. Hahn, "Analytic equation to energy conversion between electromagnetically coupled superconducting and copper coils," *Prog. Supercond. Cryogenics (PSAC)*, vol. 21, no. 1, pp. 36–39, 2019, doi: 10.9714/psac.2019.21.1.036.

[30] S. An, K. Choi, S. Noguchi, C. Im, J. Bang, U. Bong, J. Kim, and S. Hahn, "A feasibility study on 'magnetic dam' to absorb magnetic energy in NI HTS magnet during quench," *IEEE Trans. Appl. Supercond.*, vol. 30, no. 4, pp. 1–5, Jun. 2020, doi: 10.1109/TASC.2020.2972221.

[31] L. Qin, J. Liu, L. Wang, K. Wang, B. Zhou, Y. Wang, and Q. Wang, "A novel pragmatic magnetic dam structure for ultra-high field (> 27 T) superconducting magnet," *J. Supercond. Nov. Magn.*, vol. 35, no. 5, pp. 1483–1489, 2022.

[32] M. Daibo, S. Fujita, M. Haraguchi, Y. Iijima, M. Itoh, and T. Saitoh, "Development of a 5T 2G HTS magnet with a 20-cm-diameter bore," *IEEE Trans. Appl. Supercond.*, vol. 23, no. 3, Jun. 2013, Art. no. 4602004, doi: 10.1109/TASC.2013.2246758.

[33] S. Noguchi, T. Imai, D. Park, S. Hahn, and Y. Iwasa, "A simple screening current simulation method using equivalent circuit model for REBCO pancake coils," *Superconductor Sci. Technol.*, vol. 33, no. 11, Nov. 2020, Art. no. 115005, doi: 10.1088/1361-6668/abb35b.

YOJONG CHOI was born in Yeosu, South Korea, in 1990. He received the Ph.D. degree in electrical and electronic engineering from Yonsei University, Seoul, South Korea, in 2020. He is currently a Senior Researcher with the Korea Basic Science Institute, Daejeon, South Korea. His current research interests include circuit signal processing and control systems, superconducting magnets, and cryogenic systems.

SEUNGHYUN SONG was born in Seoul, South Korea, in 1986. He received the Ph.D. degree in electrical and electronic engineering from Yonsei University, Seoul, in 2018.

Following his graduate studies, he has been a Senior Researcher with the Korea Basic Science Institute, Daejeon, South Korea. His current research interests include signal processes and superconducting systems.

MYUNG SU KIM received the B.S. degree in material engineering from Chungnam National University, Daejeon, South Korea, in 2008. He is currently a Researcher with the Korea Basic Science Institute. His current research interests include the thermal properties of materials at low-temperature and the development of the electromagnetic properties measurement instrument.

JAE YOUNG JANG received the B.S., M.S., and Ph.D. degrees in electrical and electronic engineering from Yonsei University, Seoul, in 2007, 2009, and 2013, respectively. He is currently an Assistant Professor with the School of Electrical, Electronics and Communication Engineering, Korea University of Technology and Education, where he is developing superconducting magnets and control/measuring system for scientific instruments. His current research interests include superconducting magnet systems, finite element method analysis, and control/instrumentation systems.

YEON SUK CHOI received the Ph.D. degree in mechanical engineering from Florida State University, Tallahassee, in 2004. He is currently a Principal Researcher with the Korea Basic Science Institute, Daejeon, South Korea. His current research interests include the development of property measuring equipment, heat and mass transfer at low-temperature, superconducting magnet application, and mechatronic systems.